Rheological properties of Mg2SiO4 glass: A molecular dynamics study

Valentin Delbecq, Philippe Carrez, Patrick Cordier

▶ **To cite this version:**

Valentin Delbecq, Philippe Carrez, Patrick Cordier. Rheological properties of Mg2SiO4 glass: A molecular dynamics study. Journal of Non-Crystalline Solids, 2023, Journal of Non-Crystalline Solids, 619, pp.122572. 10.1016/j.jnoncrysol.2023.122572 . hal-04189371

HAL Id: hal-04189371
https://hal.univ-lille.fr/hal-04189371

Submitted on 28 Aug 2023

HAL is a multi-disciplinary open access archive for the deposit and dissemination of scientific research documents, whether they are published or not. The documents may come from teaching and research institutions in France or abroad, or from public or private research centers.

L'archive ouverte pluridisciplinaire **HAL**, est destinée au dépôt et à la diffusion de documents scientifiques de niveau recherche, publiés ou non, émanant des établissements d'enseignement et de recherche français ou étrangers, des laboratoires publics ou privés.

Distributed under a Creative Commons Attribution - NonCommercial - NoDerivatives 4.0 International License

Journal of Non-Crystalline Solids 619 (2023) 122572

Contents lists available at ScienceDirect

Journal of Non-Crystalline Solids

journal homepage: www.elsevier.com/locate/jnoncrysol

Rheological properties of Mg_2SiO_4 glass: A molecular dynamics study

Valentin Delbecq [a], Philippe Carrez [a,*], Patrick Cordier [a,b]

[a] Univ. Lille, CNRS, INRAE, Centrale Lille, UMR 8207 - UMET - Unité Matériaux et Transformations, F-59000 Lille, France
[b] Institut Universitaire de France, Paris, France

ARTICLE INFO

Keywords:
Silicate glass
Olivine
Mechanical properties

ABSTRACT

We report an initial investigation of the rheology of Mg_2SiO_4 glass through classical molecular dynamics simulations. We performed simple shear tests at different temperatures (1–300 K), shear rates (10^8–10^{10} s^{-1}) and pressures (0–10 GPa), from which we investigate the atomic rearrangements induced by loading. At low strain, atomic rearrangements, as detected by a non-affine displacement criteria, nucleate randomly in the glass. They then give rise to the formation of shear bands once the steady state of plastic flow is reached. We show that the flow stress follows a Herschel-Buckley law modified to account for the thermal activation of plastic events.

1. Introduction

Silicate glasses usually refer to amorphous materials in which SiO_2 forms a network of corner-sharing tetrahedra. These vitreous phases can further incorporate different cations leading to the well-known categories of borosilicate glasses, aluminosilicate glasses or soda-lime glasses. The intrinsic capability of amorphous materials to accommodate numerous elements make them excellent candidates for a large range of applications. As an example, complex silicate glasses have been extensively studied for their ability to sequester radioactive elements (see for instance [1–3]).

In this study, we focus on a peculiar silicate glass of composition Mg_2SiO_4. This material corresponds to the amorphous state of crystalline forsterite, the magnesium end-member of olivine $(Mg,Fe)_2SiO_4$. Compared to the silicate glasses mentioned above, where SiO_2 is the dominant oxide, in amorphous olivine, the amount of MgO is much greater which may explain why olivine melts are hardly quenchable into an amorphous state without ultra-fast quenching [4–6]. Nevertheless, this amorphous state is naturally found in primitive interstellar dust (see for instance [7]) or in meteorites [8]. The natural occurrence of Mg_2SiO_4 glass with a known poor-glass forming ability results on one hand from the amorphization of olivine crystals under ion irradiation [9,10] or on the other hand from amorphization under shock or high stress [8,11,12]. Most recently, amorphous olivine phase was discovered at grain boundaries in olivine polycrystals submitted to deformation experiments under high stress [13]. Moreover, it has been suggested that this amorphous state can play a crucial role in the mechanical behaviour of olivine polycrystals by promoting the grain boundary sliding. The mechanical properties of amorphous olivine are thus becoming of great interest in geology as it may enhanced the ductility of polycrystalline olivine at the lithosphere-asthenosphere boundary in the Earth's interior [13].

Activation of mobility of boundaries containing a glassy phase may be counter intuitive since amorphous materials, or glasses, are generally known to be fragile, suffering of shear localization and brittle failure at low temperature. However, it is now well documented that such behaviour can be suppressed with amorphous material sustaining plastic flow at microscale ([14] and references therein). Numerous examples of this plastic mechanical behaviour have been reported over the years in various glassy systems, in silica glasses [15,16], amorphous oxides [17], metallic glasses [18–20]. Micrometric samples of silica glass can be plastically deformed [16] and silicate glasses also undergo plastic deformation in similar conditions with the appearance of shear bands [21]. In case of amorphous olivine phase, Baral et al. [22] have documented a viscoelastic-viscoplastic behaviour of thin film deposited by pulsed laser deposition.

More generally, interest in the mechanical properties of glass is motivated by the potentially interesting mechanical properties expected from amorphous phases. Indeed, amorphous materials generally exhibit significantly higher strengths than their crystalline counterparts. The mechanism of plastic deformation in amorphous system involves accommodation of strain at the atomic level with rearrangement of atoms. Two models have been initially proposed to describe these atomic motions: the Shear Transformation Zone (STZ) by Argon [23] and the "free-volume" model adapted to glass deformation by Spaepen [24]. Despite the differences between the two approaches, the atomic scale

* Corresponding author.
E-mail address: philippe.carrez@univ-lille.fr (P. Carrez).

https://doi.org/10.1016/j.jnoncrysol.2023.122572
Received 15 June 2023; Received in revised form 26 July 2023; Accepted 12 August 2023
Available online 18 August 2023
0022-3093/© 2023 The Authors. Published by Elsevier B.V. This is an open access article under the CC BY-NC-ND license (http://creativecommons.org/licenses/by-nc-nd/4.0/).

mechanisms share some common features, amongst those, one finds that both are thermally activated with similar energy scales and strength. Without adhering to either model, it seems nevertheless that the STZ model has attracted increasing attention [20] and is now fully supported by atomistic simulations (see for instance [25]).

The goal of the present study is therefore to analyse the mechanical response and rheological behaviour of an olivine glass of forsterite composition Mg_2SiO_4 and to elucidate how local atomic rearrangements evolve in the deformation process at low temperature. Since the rheological behaviour of this silicate composition may be of interest in the context of the Earth's interior, it is studied in a pressure range 0–10 GPa (i.e. the range of pressure expected in the Earth's upper mantle). To this end, we have performed molecular dynamics (MD) simulations for this specific composition and analysed the atomic rearrangement events in term of STZs.

2. Computational methods

Since the atomic bonds should be similar in crystallised material and its amorphous polymorph, differing only in the arrangement of the bonds in space, we rely on the rigid-ion interatomic potentials proposed by Pedone et al. [26] for the ternary Mg, Si, O system. These interatomic potentials have been shown to accurately reproduce the physical properties of forsterite [27]. The formulation used here therefore corresponds to partial ion charges interacting via the classical long-range coulombic term, combined with short-range interactions described by a Morse function and a truncated Lennard–Jones function accounting for repulsion. MD simulations are performed with the LAMMPS code [28] using the as-implemented particle- particle-mesh (pppm) method to compute the coulomb terms. Throughout this study, we investigate a stoichiometric Mg_2SiO_4 compound and most of the calculations presented below have been performed on a cubic-shaped system ($14.9 \times 14.7 \times 14.8$ nm^3 at zero pressure, later decreased by 9% and 14% at 5 and 10 GPa of applied pressure) containing 282,240 atoms, although smaller system sizes have also been investigated to exclude any finite size effects.

The Mg_2SiO_4 glass is obtained from a liquid heated to 3300 K and then quenched at a quench rate of 100 K.ps^{-1}. We used a thermostat and a barostat of Nose-Hoover type to control both P and T conditions during linear quenching. The as-quenched configurations are then heated to the temperature of interest and equilibrated for 20 ps. The equilibrated configuration is finally stabilised using a NVT ensemble before being subjected to a simple shear loading γ_{xy} (at constant shear rate). In the following, we consider a temperature range from 1 K to 300 K and shear rates from 10^{10} s^{-1} down to 10^{8} s^{-1}. For calculations performed at 5 and 10 GPa, we have limited our simulations of shear experiments to a shear rate of 10^{9} s^{-1}.

In order to analyse the atomic rearrangements that occur during plastic deformation of the glass, we use the criteria proposed by Falk & Langer [29], now called D^2_{min} non-affine displacement. This quantity quantifies the substantial deviation of molecular displacements in a time interval Δt with respect to what can be expect from a linear strain field. For a central atom i, the mean square difference D^2 is calculated according to Eq. (1).

$$D^2(i) = \frac{1}{N}\sum_j \left(\overrightarrow{r_{ij}(t)} - J_i\overrightarrow{r_{ij}(t-\Delta t)}\right)^2 \quad (1)$$

Where $r_{ij} = r_j - r_i$, is the vector between the central atom i and its neighbours j, selected in a sphere of N nearest neighbours. r_{ij} is then computed at times t and t-Δt, and D^2 is calculated according to the local affine transformation tensor J_i. D^2 is thus minimised, and quoted as D^2_{min}, as the residual of the least squares fit by which J_i is quantified. In what follows, it can be seen that the time interval Δt is equivalent to a strain interval $\Delta\gamma$ since shear loading is performed at a fixed shear rate. Finally, atomic configurations are visualised using OVITO software [30].

3. Results

3.1. Mg_2SiO_4 glass structure

The isotropic radial distribution function $g(r)$ of Mg_2SiO_4 glass at zero pressure is shown in Fig. 1. With broad neighbouring peaks, the $g(r)$ function is typical of a disordered system. The first three peaks correspond to Si-O, Mg-O and O—O bonds respectively (see also the partial bond distribution functions given in Supplementary Fig. 2). The first peak, corresponding to Si-O bonds, is centred around 1.6 Å, i.e. a bond length similar to the length of the same bond in the crystalline forsterite structure (computed with the same potential). Indeed, in the amorphous phase, Si is found inside O tetrahedra similar to those in the forsterite structure. Moreover, as in conventional silicate glasses [31], most SiO_4 tetrahedra share oxygen corner atoms, but without developing a true glass forming network [5,32]. Indeed, around a quarter of SiO_4 tetrahedra remains isolated as a single entity, in agreement with the proportion of unconnected tetrahedra reported in [32]. The peak of Mg-O's first neighbours, located around 2.0 Å, gives a slightly asymmetric distribution with bond distances between 1.8 and 2.4 Å, reflecting the tendency of Mg cations to be located in a variety of polyhedra environments. This is confirmed by the broadening of the following O—O bonds peaks, reflecting the possibility of various coordinations in the glass. The local coordination of Mg corresponds to MgO_4, MgO_5 and MgO_6 octahedra (as in the crystal state). However, the shift of the Mg-O peak to the smaller distances indicates a strong tendency for MgO polyhedra to relax mainly into MgO_4 or MgO_5 units. Such a mixture of polyhedral magnesium environments is consistent with the rare experimental characterizations of forsterite glasses (see for instance [6]). The glass structures obtained at 5 and 10 GPa are broadly identical to those described above (as shown in Supplementary Fig. 1). The average distances of the Si-O and Mg-O bonds are not radically affected by the applied pressure, suggesting that the distances of the cationic first neighbours result mainly from the definition of the pairwise potential used. The effect of pressure is only evidenced for O—O bonds for which a slight shift toward the smallest distances is observed.

3.2. Mechanical properties

The mechanical properties of Mg_2SiO_4 glass are investigated by subjecting the system to simple shear deformations. Fig. 2 illustrates the different stress-strain curves recorded at different shear rates and temperatures for calculations at zero pressure. Note that each curve result from the average of five different MD runs conducted up to a total strain of 1. The stress-strain curves show the typical mechanical response of a

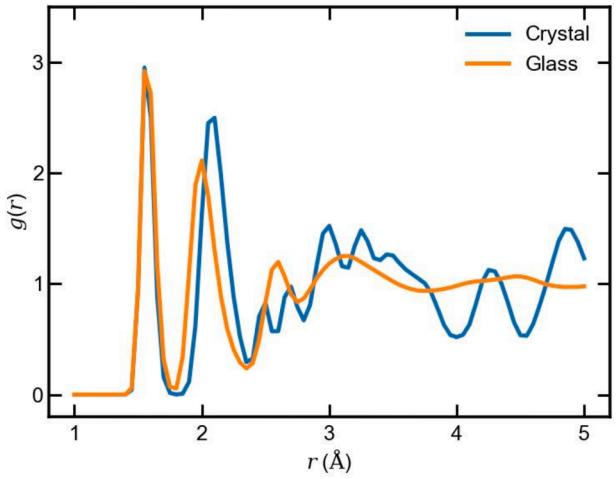

Fig. 1. Radial distribution function $g(r)$ at 300 K and zero pressure of as-quenched Mg_2SiO_4 glass and crystal.

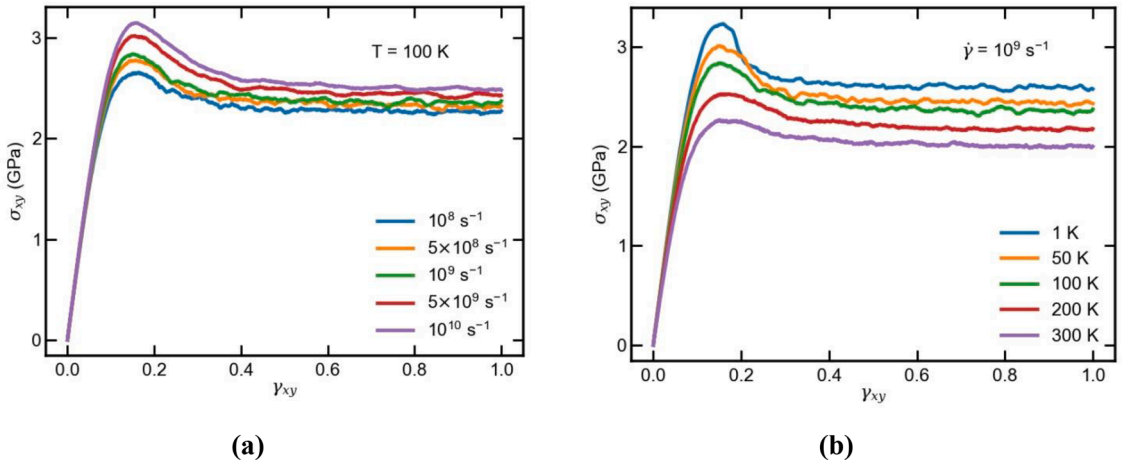

Fig. 2. Simple shear, stress-strain curves calculated at zero pressure. (a) Effect of shear rates for calculations performed at 100 K. (b) Effect of temperature for calculations performed at 10^9 s^{-1}.

glassy material, i.e. a linear portion, followed by a yield point before a rapid decrease of stress leading to a steady-state flow at a constant stress.

The linear regime, observed in the first part of the stress-strain curves and assumed to correspond to an elastic behaviour, makes it possible to determine a shear modulus which appears to be rather insensitive to strain rate and decreasing with temperature from 34 GPa to 28 GPa at 300 K. In the temperature and strain rate range studied here, the yield point occurs at a strain $\gamma \sim 0.15$. Above this, we observe a flow at constant stress punctuated by stress drops. On average, this steady state stage ($0.5 \leq \gamma \leq 1.0$) allows us to define a flow stress associated with both strain rate and temperature conditions which are summarised in Fig. 3. We find that the flow stress depends on strain-rate and temperature. Low strain-rates are associated with low flow stress values and, simultaneously, a significant decrease of the flow stress is observed at high temperature. For a constant shear rate of 10^9 s^{-1}, we repeated these calculations at pressures of 5 and 10 GPa (see an example at 300 K in Fig. 4,a). It can be seen that pressure affects the stress levels reached at the yield and also during flow (Fig. 4,a), but overall, temperature still produces a significant decrease in flow stress (Fig. 4,b).

3.3. Microstructural characterization

To visualise the clusters of atoms that undergo local rearrangements during shear, we rely on the D^2_{min} criterion mentioned in Section 2. To calculate D^2, we use a neighbouring sphere of 5 Å which, according to the $g(r)$ function shown in Fig. 1, allows us to take into account the different types of bonds. Considering a time interval Δt defined from the starting point of the simulation ($t = 0$ and no applied strain), we can visualise the cumulative local strains as a function of the time elapsed since the start of the deformation test, i.e. as a function of the strain-state of the system. Fig. 5 (a,b,c,d) shows a series of snapshots of this cumulative quantity for a typical simulation. It clearly shows that a shear band develops during the simulation, which tends to thicken as the strain increases. Instead of mapping the cumulative nonaffine displacement, we can reduce the time interval to analyse local events within a narrow strain window. However, the interval time Δt, or equally speaking the strain interval $\Delta\gamma$ must be chosen in such a way that the system evolves in a diffusive regime. In other words, the time interval must be greater than or close to the β-relaxation time of the system [33]. To satisfy this condition, we have chosen a time interval corresponding to a strain window $\Delta\gamma$ of 0.06. We further verified by computing the mean squared displacement (MSD) (here only along the z direction to avoid any bias due to the application of shear) as a function of the applied strain, that beyond a strain of 0.05, the MSD was indeed greater than the distance r^2 of the first neighbours, and characteristic of a significant atomic displacement. Fig. 5 (e,f,g,h) show how individual, localised events are distributed in the system. At small strain, Fig. 5 (e,f), we observe individual events randomly distributed throughout the volume. At larger strain, we note an evolution of the spatial distribution of the events associated with the development of the shear band. Fig. 5,h shows that localised events of different sizes tend to be concentrate in the shear band.

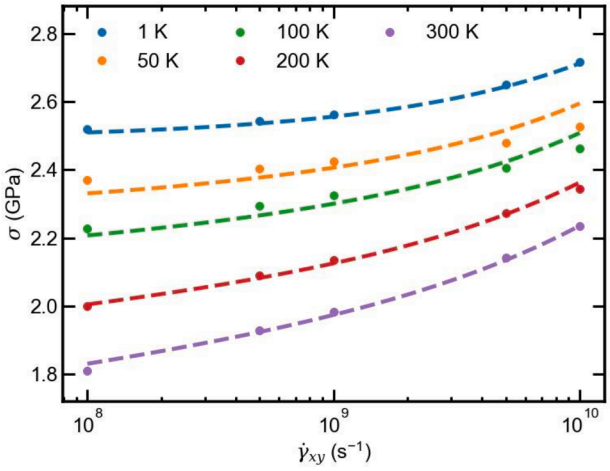

Fig. 3. Flow stress σ as a function of shear rates $\dot{\gamma}$ for all calculations performed at zero pressure. The lines correspond to a fit of the MD data obtained using Eq. (2).

Fig. 6 shows the probability distribution of D^2_{min}, which describes the intensity of local atomic rearrangements associated with localised events. The probability distributions tend to exhibit common characteristics, irrespective of the temperature or the strain at which they were recorded. All distributions are indeed characterised by high probabilities at low intensity and a long tail at higher D^2_{min}. Fig. 6,a shows that as strain increases, the distributions shift toward high D^2_{min} values before collapsing into a typical distribution curve in the steady plastic flow regime. We also note (Fig. 6,b) that temperature tends to reduce the extend of the distribution, favouring the appearance of higher intensity events. Interestingly, high intensity events are often calculated within a cluster of atoms centred on a Mg atom. Indeed, half of the highest D^2_{min} intensity events correspond to a calculation of D^2 around a central Mg atom, whereas for these high intensity events, we found only 1% of these events calculated around a Si atom. Conversely, low intensity events tend to be associated with an over-representation of Si (relative to a stoichiometric proportion) as the central atomic species, since Si or Mg

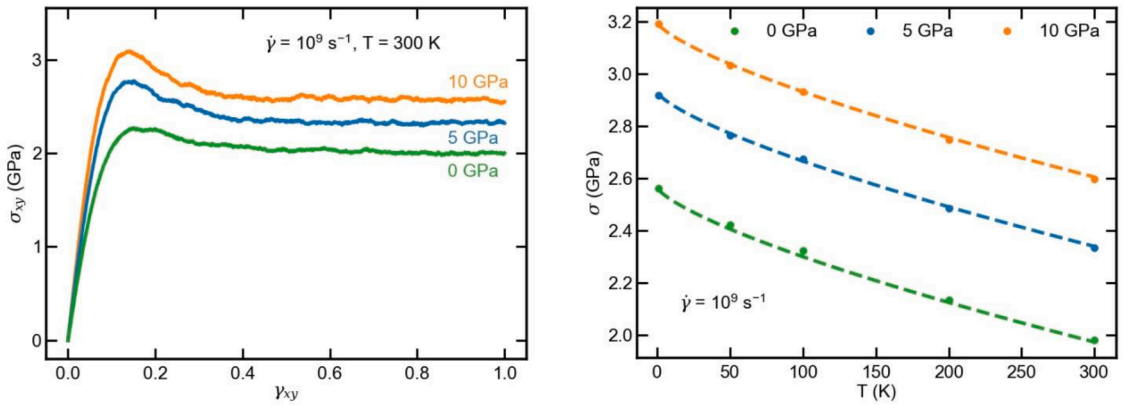

Fig. 4. (a) Simple shear stress-strain curves ($\dot{\gamma}$= 10^9 s^{-1}) calculated at 300 K for three different pressures. (b) Flow stress σ plotted against temperature for three pressures and $\dot{\gamma}$= 10^9 s^{-1}. The lines correspond to the fit obtained using Eq. (2). Note that parameters a_2 and a_3 in Eq. (2) corresponding to the contribution of thermal activation are held constant with a well-captured prediction of $T^{2/3}$ flow stress behaviour with pressure.

corresponds to the centre of the event in the same proportion of 20% of the lowest intensity events.

To go a step further, we also studied the spatial correlation of the non-affine displacements *C(r)*. To do this, we used the spatial auto correlation function proposed by Jana & Pastewa [33]. Fig. 7,a shows some examples of the D^2_{min} correlation functions calculated at different strains. From the decay of *C(r)*, we define a characteristic length l_c based on an exponential decay exp(-*r*/l_c), since the correlation function has a linear slope in the logarithmic graph (Fig. 7,a). Fig. 7,b summarises the evolution of l_c as a function of strain for the different deformation temperatures investigated here at zero pressure. The evolution of l_c shows two different behaviours before and after the establishment of the shear band. While, in the elastic part of the stress – strain curve (below γ ~ 0.15), the correlation length is small, it increases considerably around the yield strain and tends to reach a fixed high value during the plastic regime. This phenomenon is noticeable at low temperature (below 200 K). However, at higher temperatures, and for larger values of strain, we observe a decrease in l_c. It is worth noticing that the evolution of the characteristic length described above is identical to those recorded during shear deformation simulations performed at 5 and 10 GPa (as shown Supplementary Fig. 5).

4. Discussion

Shear induced irreversible atomic arrangements and their relationship to the mechanical behaviour of amorphous solids have been extensively studied in various types of systems ([34] and references therein). The behaviour of Mg_2SiO_4 glass revealed in this study is consistent with the typical mechanical response of metallic glasses [20] and viscoplastic solids [35]. At low strain, the linear relationship between stress and strain enabling us to measure a shear modulus independent of the strain rate, suggesting a reversible elastic behaviour. Plastic flow occurs at higher strains, beyond a yield point. The shape of the stress-strain curves depends on both strain-rate and temperature, but it should be remembered that the yield stress should also be sensitive to glass preparation [36–38]. This characteristic will not be addressed later, as sample preparation was not specifically investigated here. The maximum stress at yield, the flow stress, but also the various stress drops observed on the stress-strain curves are macroscopic evidence of the activation of plastic events [34,38,39] during our simulations. Since the stress-strain curves shown in Fig. 2 or 4 were averaged over five independent simulations, the punctuation of the curves by numerous stress drops may, to some extent, only be visible during the plastic flow regime, even if stress drops occur before this stage (as shown in Supplementary Fig. 3).

Localised atomic rearrangements within the STZ produce plastic strain and end up ordering themselves into shear bands. In case of Mg_2SiO_4 glass, Fig. 5 shows that localised events of different sizes tend to coalesce to form the shear band. Our observations are therefore consistent with what is known in different systems such as metallic glasses [20,40], for instance, or amorphous silica [21]. However, the shear band that appear in our MD simulations cannot be considered as a permanent shear band but rather as an elementary shear band that results from an avalanche of localised events of different sizes [14]. The appearance of the shear band begins at a strain around the yield point which is a fairly ubiquitous feature of strain-controlled simulations, irrespective of the amorphous solid under study [34,39]. Above this point, the system enters a flow regime typical of an elastoplastic steady state and all plastic events distributions (Fig. 6) tend to collapse into a typical distribution. Such a behaviour has already been reported in metallic glasses (e.g. [37]).

In order to quantify the characteristic length scales of STZs, one can rely on the analysis of the spatial correlation function *C(r)*. It is indeed convenient to use the characteristic length l_c of the exponential decay of *C(r)* as a measure of the STZ size [33,40]. However, depending on the strain state of the system, l_c which provides a measure of cooperative atomic motions, can be interpreted as reflecting individual STZs or as reflecting the behaviour of the shear band [33]. Specifically, above the yield strain, l_c can be interpreted as a measure of the distance between replicated shear bands (as a consequence of the use of periodic boundary conditions). This therefore explains the decrease in l_c observed at high temperature (here 200 K and 300 K, Fig. 7,b). As the strain increases, the shear band being thicker, this distance decreases as the shear band fills the entire volume. Such behaviour is expected to occur at lower temperatures, but at strains greater than 1.0, which is not illustrated here. Nevertheless, prior to yield, l_c should be a good indicator of the size of an individual STZ, since we observe no shear band development and a random distribution of localised events. It turns out that in Mg_2SiO_4 glass, STZs are characterised by a size of ~ 5 Å (involving ca. 20 atoms). Due to the limited range of strain accessible for measuring STZ size, it is difficult to estimate if the size of STZs differs for the different ranges of temperature or pressure investigated in this study.

As with other amorphous solids, in Mg_2SiO_4 glass we show that the effect of temperature decreases flow stress, while increasing shear rate tends to contribute positively to the flow stress (at least in the range of shear loading rates considered here with MD simulations). The combined effect of temperature and strain rate has been extensively studied (see, for instance, review [34]). It is generally assumed that one effect of temperature is to favour the involvement of more atoms in irreversible rearrangements, leading to a decrease in the flow stress [37]. This

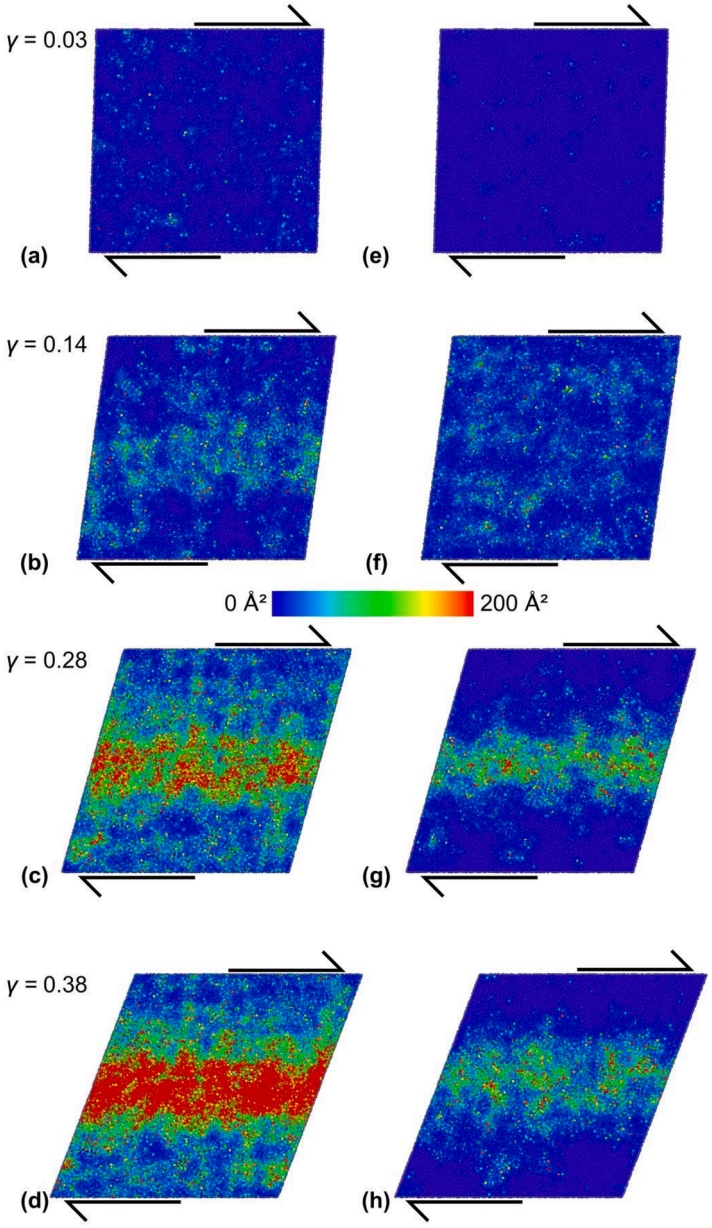

Fig. 5. Series of snapshots of the atomic configuration of Mg_2SiO_4 glass deformed at zero pressure and 100 K with a strain-rate $\dot{\gamma}= 10^9$ s^{-1}. Atoms are coloured according to D^2_{min} intensity calculated from a cumulative perspective (a)-(d) or using a strain window of 0.06 (e)-(h) to highlight the distribution of localized events (see text for details).

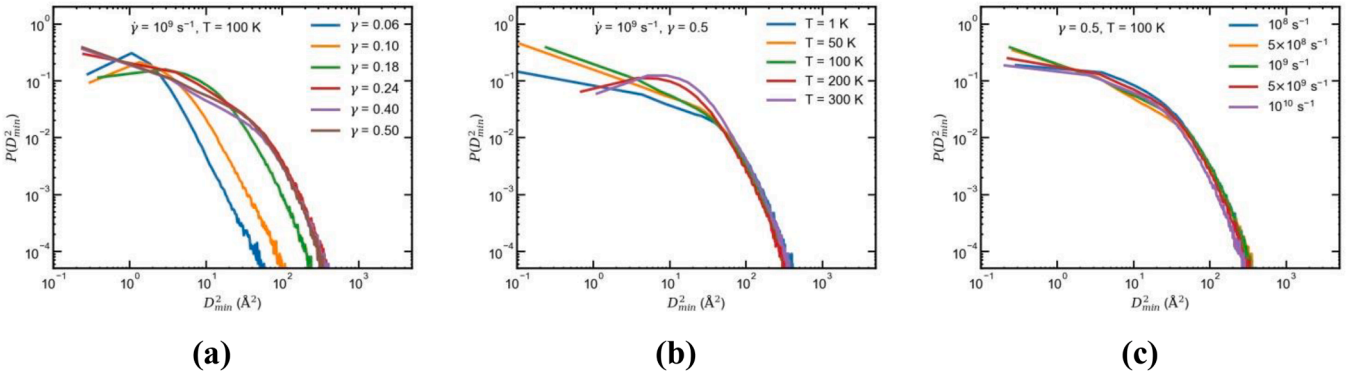

Fig. 6. Probability distribution of D^2_{min} shown here for calculations at zero pressure. (a) Distribution plotted as a function of strain γ for a calculation performed at 100 K using a shear rate of 10^9 s^{-1}. Effect of temperature (b) and strain rate (c) on the distribution for a strain of 0.5.

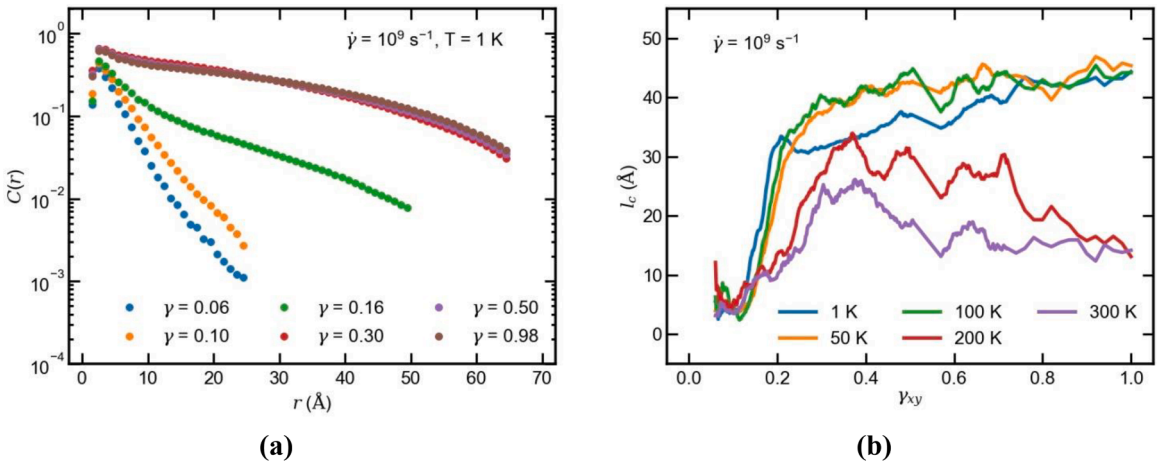

Fig. 7. (a) Spatial correlation function $C(r)$ measured at different strain values in a shear experiment performed at 1 K and $\dot{\gamma}$=10^9 s^{-1}. (b) Evolution of the characteristic correlation length l_c as a function of shear strain γ for different temperatures and a shear rate of 10^9 s^{-1}.

hypothesis is supported in our case by the evolution of the D^2_{min} distribution as a function of temperature (Fig. 6) for which we count more high intensity events as temperature increases. With respect to the loading rate, the increase in flow stress is interpreted in terms of dynamic effects for which the time required for atomic relaxation will be not met at extremely high rates [41,42]. This consideration may explain why we recorded irreversible events centred on Mg atoms with little representation of Si atoms. Indeed, in Mg_2SiO_4 glass, which is inhomogeneous at the atomic local scale, Si atoms can be expected to be more strongly bound within SiO_4 tetrahedra, thus reducing their relaxation capacity relative to the other cations.

Overall, our results suggest that an interplay between, temperature and strain rate can describe the rheological behaviour in Mg_2SiO_4 glass. To test this hypothesis, we rely on the universal expression of Herschel-Bulkley (HB) form proposed by Chattoraj et al. [42]. Based on a physical description of transformation zones activated by mechanical loading but enhanced by temperature, it allows us to combine strain-rate and temperature in a Herschell-Buckley-type expression of the following form Eq. (2):

$$\sigma(\dot{\gamma},T) = a_0 + a_1 \times \dot{\gamma}^m - a_2 T^{\frac{2}{3}} \times \left(\ln\left(\frac{a_3 T^{\frac{5}{6}}}{\dot{\gamma}}\right)\right)^{\frac{2}{3}} \quad (2)$$

where $\sigma(\dot{\gamma},T)$ corresponds to the flow stress derived from our MD simulations for a given $\dot{\gamma}$ and T. a_0, a_1, a_2, a_3 and m are constants. Fitting these constants to our zero pressure data leads to a unique set of parameters (Table 1) that reproduce with satisfactory accuracy all the calculations performed here as shown in Fig. 3. In this generalised Herschel-Bulkley equation, a_0 can be interpreted as the flow stress in athermal quasistatic conditions (here 2.5 GPa for a glass quenched at zero pressure) and we find m~0.54. The last term of the expression corresponds to the deviation from the classical Herschel-Bulkley law due to thermal activation [42]. Interestingly, such a deviation fitted at zero pressure almost perfectly predicts the behaviour of the glass deformed at 5 and 10 GPa (Fig. 4,b). The effect of pressure in our simulations is only taken into account by the athermal quasistatic stress a_0 which increases with increasing pressure.

Table 1
Parameters of Eq. (2) as deduced from the fit of MD flow stress data. Note that the predictions of Eq. (2) with respect to the MD data computed at 5 and 10 GPa require the adjustment of the athermal quasistatic stress a_0.

	Pressure		
	0 GPa	5 GPa	10 GPa
a_0 (GPa)	2.50	2.87	3.13
a_1 (GPa.s^{-m})	8 10^{-7}		
M	0.54		
a_2 (GPa.K$^{3/2}$)	31 10^{-4}		
a_3 (s.K$^{6/5}$)	53.3 10^9		

Due to the experimental difficulty of quenching glass of Mg_2SiO_4 composition, there are few data available for comparison with our calculations. Recently, Baral et al. [22] carried out indentation relaxation tests on thin amorphous olivine films obtained by pulsed laser deposition. They analysed their data with a power-law with a strain-rate sensitivity equal to ~ 0.05 corresponding to strain-rates in the range 10^{-6} – 10^{-4} s^{-1}. On the basis of our generalised Herschel-Bulkley equation, our results can be extrapolated to the range of experimental strain-rates used in [22]. If analysed with a power-law, they yield a strain rate sensitivity between 0.04 and 0.05 for T = 300 K and 350 K respectively. Far from being perfect, the agreement between the extrapolation of our results and the measurements of [22], is fair considering that the rheological behaviour can be affected by several parameters like quench rate, glass preparation or ageing.

5. Concluding remarks

In summary, we have studied the mechanical response of Mg_2SiO_4 glass under simple shear conditions. MD simulations enable us to relate the atomic rearrangements and their spatial distribution to the evolution of the glass's stress-strain response. The mechanical properties of Mg_2SiO_4 glass follow the fairly universal pattern of the stress-strain dependence of amorphous solids, with two distinct regions. At low strain, a linear stress-strain relationship is observed on average, which then evolves into a steady-state regime with a constant flow stress punctuated by plastic events. Microscopic characterizations show that Mg_2SiO_4 glass plastically deforms with STZs a few angstroms in size. The flow stress of Mg_2SiO_4 glass follows a Herschel-Bulkley law modified to account for the thermal activation of STZ's. We also show that the temperature dependence added to the Herschel-Bulkley equation is insensitive to applied pressure up to 10 GPa.

Credit author statement

All authors listed have made a significant contribution to the research reported and have read and approved the submitted manuscript, and furthermore, all those who made substantive contributions to this work have been included in the author list.

Declaration of Competing Interest

The authors declare that they have no known competing financial interests or personal relationships that could have appeared to influence the work reported in this paper.

Data availability

Data will be made available on request.

Acknowledgements

This work has received funding from the European Research Council (ERC) under the European Union's Horizon 2020 research and innovation programme under grant agreement no 787198 – TimeMan. Computational resources have been provided by the DSI at Université de Lille.

Supplementary materials

Supplementary material associated with this article can be found, in the online version, at doi:10.1016/j.jnoncrysol.2023.122572.

References

[1] I.W. Donald, B.L. Metcalfe, R.N.J. Taylor, The immobilization of high level radioactive wastes using ceramics and glasses, J. Mater. Sci. 32 (1997) 5851–5887, https://doi.org/10.1023/A:1018646507438.
[2] W.E. Lee, M.I. Ojovan, M.C. Stennett, N.C. Hyatt, Immobilisation of radioactive waste in glasses, glass composite materials and ceramics, Adv. Appl. Ceram. 105 (2006) 3–12, https://doi.org/10.1179/174367606X81669.
[3] S. Gin, J.M. Delaye, F. Angeli, S. Schuller, Aqueous alteration of silicate glass: state of knowledge and perspectives, npj Mater. Degrad. 5 (2021) 42, https://doi.org/10.1038/s41529-021-00190-5.
[4] P. Richet, F. Leclerc, L. Benoist, Melting of forsterite and spinel, with implications for the glass transition of Mg_2SiO_4 liquid, Geophys. Res. Let. 20 (1993) 1675–1678, https://doi.org/10.1029/93GL01836.
[5] J.A. Tangeman, B.L. Philips, A. Navrotsky, J.K. Richard Weber, A.D. Hixson, T. S. Key, Vitreous forsterite, (Mg_2SiO_4): synthesis, structure, and thermochemistry, Geophys, Res. Let 28 (2001) 2517, https://doi.org/10.1029/2000GL012222. -1520.
[6] M.C. Wilding, C.J. Benmore, J.A. Tangeman, S. Sampath, Coordination changes in magnesium silicate glasses, Europhys. Lett. 67 (2004) 212–218, https://doi.org/10.1209/epl/i2003-10286-8.
[7] F.J.M. Rietmeijer, the irradiation-induced olivine to amorphous pyroxene transformation preserved in an interplanetary dust particle, Astrophys. J. 705 (2009) 791–797, https://doi.org/10.1088/0004-637X/705/1/791.
[8] R. Jeanloz, T.J. Ahrens, J.S. Lally, G.L. Nord, J.M. Christie, A.H. Heuer, Shock-produced olivine glass: first observation, Science 197 (1977) 457–459. http://www.jstor.org/stable/1744975.
[9] K. Demyk, P. Carrez, H. Leroux, P. Cordier, A.P. Jones, J. Borg, E. Quirico, P. I. Raynal, L. D'Hendecourt, Structural and chemical alteration of crystalline olivine under low energy He+ irradiation, A&A 368 (2001) L38–L41, https://doi.org/10.1051/0004-6361:20010208.
[10] J.R. Brucato, G. Strazzulla, G. Baratta, L. Colangeli, Forsterite amorphisation by ion irradiation: monitoring by infrared spectroscopy, A&A 413 (2004) 395–401, https://doi.org/10.1051/0004-6361:20031574.
[11] D. Andrault, M.A. Bouhifd, J.P. Itié, P. Richet, Compression and amorphization of (Mg,Fe)2SiO4 olivines: an X-ray diffraction study up to 70 GPa, Phys. Chem. Minerals 22 (1995) 99–107, https://doi.org/10.1007/BF00202469.
[12] K. Kranjc, A.S. Thind, A.Y. Borisevich, R. Mishra, K.M. Flores, P. Skemer, Amorphization and plasticity of olivine during low-temperature micropillar deformation experiments, J. Geophys. Res. Solid Earth. 125 (2020) 0–3, https://doi.org/10.1029/2019JB019242.
[13] V. Samae, P. Cordier, S. Demouchy, C. Bollinger, J. Gasc, S. Koizumi, A. Mussi, D. Schryvers, H. Idrissi, Stress-induced amorphization triggers deformation in the lithospheric mantle, Nature 591 (2021) 82–86, https://doi.org/10.1038/s41586-021-03238-3.
[14] A. Tanguy, Elasto-plastic behavior of amorphous materials: a brief review, C R Phys 22 (2021) 117–133, https://doi.org/10.5802/crphys.49.
[15] J.D. Mackenzie, High-pressure effects on oxide glasses: I, densification in rigid state, J. Amer. Ceram. Soc. 46 (1963) 461–470, https://doi.org/10.1111/j.1151-2916.1963.tb13776.x.
[16] R. Lacroix, G. Kermouche, J. Teisseire, E. Barthel, Plastic deformation and residual stresses in amorphous silica pillars under uniaxial loading, Acta Mater 60 (2012) 5555–5566, https://doi.org/10.1016/j.actamat.2012.07.016.
[17] T.M. Gross, M. Tomozawa, A. Koike, A glass with high crack initiation load: role of fictive temperature-independent mechanical properties, J. Non-Cryst. Solids 355 (2009) 563–568, https://doi.org/10.1016/j.jnoncrysol.2009.01.022.
[18] A.L. Greer, K.L. Rutherford, I.M. Hutchings, Wear resistance of amorphous alloys and related materials, Int. Mater. Rev. 47 (2002) 87–112, https://doi.org/10.1179/095066001225001067.
[19] T.C. Hufnagel, Editorial, Preface to the viewpoint set on mechanical behavior of metallic glasses, Scripta Mater. 54 (2006) 317–319, https://doi.org/10.1016/j.scriptamat.2005.10.004.
[20] C.A. Schuh, T.C. Hufnagel, U. Ramamurty, Mechanical behavior of amorphous alloys, Acta Mater. 55 (2007) 4067–4109, https://doi.org/10.1016/j.actamat.2007.01.052.
[21] T.M. Gross, M. Tomozawa, Fictive temperature-independent density and minimum indentation size effect in calcium aluminosilicate glass, J. Appl. Phys. 104 (2008), 063529, https://doi.org/10.1063/1.2985907.
[22] P. Baral, A. Orekhov, R. Dohmen, M. Coulombier, J.P. Raskin, P. Cordier, H. Idrissi, T. Pardoen, Rheology of amorphous olivine thin films characterized by nanoindentation, Acta Mater. 219 (2021), 117257, https://doi.org/10.1016/j.actamat.2021.117257.
[23] A.S. Argon, Plastic deformation in metallic glasses, Acta Metall. 27 (1979) 47–58, https://doi.org/10.1016/0001-6160(79)90055-5.
[24] F. Spaepen, A microscopic mechanism for steady state inhomogeneous flow in metallic glasses, Acta Metall. 25 (1977) 407–415, https://doi.org/10.1016/0001-6160(77)90232-2.
[25] T. Albaret, A. Tanguy, F. Boioli, D. Rodney, Mapping between atomistic simulations and Eshelby inclusions in the shear deformation of an amorphous silicon model, Phys. Rev. E 93 (2016), 053002, https://doi.org/10.1103/PhysRevE.93.053002.
[26] A. Pedone, G. Malavasi, M.C. Menziani, A.N. Cormack, U. Segre, A new self-consistent empirical interatomic potential model for oxides, silicates, and silica-based glasses, J. Phys. Chem. B 110 (2006) 11780–11795, https://doi.org/10.1021/jp0611018.
[27] P. Hirel, J. Furstoss, P. Carrez, A critical assessment of interatomic potentials for modelling lattice defects in forsterite Mg_2SiO_4 from 0 to 12 GPa, Phys. Chem. Miner. 46 (2021), https://doi.org/10.1007/s00269-021-01170-6.
[28] S.J. Plimpton, Fast parallel algorithms for short-range molecular dynamics, J. Comp. Phys. 117 (1995) 1–19. http://lammps.sandia.gov.
[29] M.L. Falk, J.S. Langer, Dynamics of viscoplastic deformation in amorphous solids, Phys. Rev. E 57 (1998) 7192–7205, https://doi.org/10.1103/PhysRevE.57.7192.
[30] A. Stukowski, K. Albe, Dislocation detection algorithm for atomistic simulations, Model. Simul. Mater. Sci. Eng. 18 (2010) 25016, https://doi.org/10.1088/0965-0393/18/2/025016.
[31] A. Retsinas, A.G. Kalampounias, G.N. Papatheodorou, Glass formation and Raman spectra of CaO-SiO2 glasses towards the orthosilicate limit, J. Phys. Chem. Solids 99 (2016) 19–24, https://doi.org/10.1016/J.jpcs.2016.08.001.
[32] S. Kohara, K. Suzuya, K. Takeuchi, C.K. Loong, M. Grimsditch, J.K.R. Weber, J. A. Tangeman, T.S. Key, Glass Formation at the Limit of Insufficient Network Formers, Science 303 (2004) 1649–1652, https://doi.org/10.1126/science.10950.
[33] R. Jana, L. Pastewka, Correlations of non-affine displacements in metallic glasses through the yield transition, J. Phys. Mater. 2 (2019), 045006, https://doi.org/10.1088/2515-7639/ab36ed.
[34] D. Rodney, A. Tanguy, D. Vandembroucq, Modeling the mechanics of amorphous solids at different length scale and time scale, Modell. Simul. Mater. Sci. Eng. 19 (2011), 083001, https://doi.org/10.1088/0965-0393/19/8/083001.
[35] S. Alexander, Amorphous solids: their structure, lattice dynamics and elasticity, Phys. Rep. 296 (1998) 65–236, https://doi.org/10.1016/S0370-1573(97)00069-0.
[36] F. Delogu, Irreversible atomic rearrangements in elastically deformed metallic glasses, Intermetallics 19 (2011) 86–92, https://doi.org/10.1016/j.intermet.2010.09.015.
[37] B.S. Shang, M.Z. Li, Y.G. Yao, Y.J. Lu, W.H. Wang, Evolution of atomic rearrangements in deformation in metallic glasses, Phys. Rev. E 90 (2014), 042303, https://doi.org/10.1103/PhysRevE.90.042303.
[38] T. Niiyama, M. Wakeda, T. Shimokawa, S. Ogata, Structural relaxation affecting shear-transformation avalanches in metallic glasses, Phys. Rev. E 100 (2019), 043002, https://doi.org/10.1103/PhysRevE.100.043002.
[39] P.K. Jaiswal, I. Procaccia, C. Rainone, M. Singh, Mechanical yield in amorphous solids: a first-order phase transition, Phys. Rev. Lett. 116 (2016), 085501, https://doi.org/10.1103/PhysRevLett.116.085501.
[40] P. Murali, Y.W. Zhang, H.J. Gao, On the characteristic length scales associated with plastic deformation in metallic glasses, Appl. Phys. Let. 100 (2012), 201901, https://doi.org/10.1063/1.4717744.
[41] Y. Shi, M.L. Falk, Strain localization and percolation of stable structure in amorphous solids, Phys. Rev. Let. 95 (2005), 095502, https://doi.org/10.1103/PhysRevLett.95.095502.
[42] J. Chattoraj, C. Caroli, A. Lemaître, Universal additive effect of temperature on the rheology of amorphous solids, Phys. Rev. Let. (2010), 266001, 10.1103/PhysRevLett.105.266001.